Journal of Computing and Electronic Information Management
ISSN: 2413-1660 | Vol. 16, No. 1, 2025

Modeling and control of shipboard power systems with inverter air conditioners for frequency regulation

Liu Yu

College of Electrical Engineering, Southwest Minzu University, Chengdu, Sichuan, 610041, PR China

Abstract: Because of the characteristics of sustainable development of renewable energy resources (RESs), the large-scale RESs are integrated into the smart grid. Nevertheless, frequency can easily fluctuate beyond the acceptable limit on account of the intermittent of RESs. In this paper, the regulation method called demand response (DR) is applying by adjusting the controllable load resources of demand side. As one of the essential loads, massive inverter air conditioners (IACs) can change their state in a short time and have little influence on user experience. Thus, it is adopted to provide frequency support in frequency regulation of shipboard microgrid (SMG) in this work. However, this also preventively introduces multiple time delays on the other hand, which result in oscillation and instability of the SMG with high probability. To handle this issue, the stability of the SMG with the participation of IACs is analysed and the delay-dependent stability criteria are further derived by employing appreciate Lyapunov-Krasovskii functional candidate, some delay-dependent techniques and linear matrix inequality method when considering single time delay and multiple time delays respectively. Then, the effect of frequency control and the comparison results of influence cause by time delay are demonstrate in different scenarios, which validates of the validity and superiority proposed method.

Keywords: Inverter air conditioner (IAC); Frequency regulation; Time delay; System stability; Demand response (DR).

1. Introduction

In the past decade, due to the massive use of fossil energy in industry, the greenhouse gas emission has dramatically increased, which has inevitably put an unbearable burden on the environment. Especially on the shipboard power systems (SPSs)[1-4], some renewable energy sources (RESs) have been introduced in order to replace the use of fossil energy, such as sea wave energy, solar energy, wind energy, etc. Compared with fossil energy, these RESs have lower cost and higher reliability, which is more conducive to efficient utilization of energy and improvement of the stability of the SPSs. However, not all of these energy sources are beneficial for the SPSs, and they can adversely affect the SPSs. This is mainly reflected in the following two aspects: high penetration of sea wave energy, solar energy and wind energy and the power loss caused by the uncertainty of illumination and wind speed. Thereupon, in order to guarantee power quality and ensure the stability of SPSs, the energy storage systems (ESSs) are generally applied .

In fact, an SPS consisted of photovoltaic cells, sea wave energy and ESSs can be referred as a specific shipboard microgrid (SMG) with the character of mobility. And some related researches have been implemented according to the application of SMG [6-8] in marine industry. In the research of , diesel generators with lithium-ion batteries are utilized to drive the cranes of ships. In the work of , the hybrid diesel/PV systems with ESS units are employed to produce environmental and economic benefits. In the study of , the issue of optimal size selection of hybrid diesel/PVC/battery power systems is discussed while neglecting the influence of the marine vessel roll. In the contribution of , the PV systems are applied for saving the fuel cost of merchant ship. In the development of , the stability analysis is conducted for hybrid diesel/PVC/battery power systems. Nevertheless, the load frequency control (LFC) issue is not involved in the above studies. It is obviously significant entry in SMGs.

When considering isolated SMG, the frequency fluctuations caused by power changes can be reduced only if RESs and ESSs can be properly coordinated. The principle is based on the compensation for unbalance of generation and demand, which is also the foundation of LFC. The main purpose of LFC are adjusting frequency of systems while saving limited fuels and prolonging the lifetime of batteries. There have various frequency regulation methods been proposed for application in LFC, such as dynamic control strategy, intelligent control strategy, adaptive control strategy, model predictive control strategy, etc. In [], a frequency control model is presented, which connect the wind farm with conventional units. Meanwhile, the active power variation value under various circumstances could be decided by the integral controller, washout filter, and the Proportional-Integral-Derivative (PID) controller. The electric vehicles are employed as diffused energy storage units to participate the smart grids frequency regulation in . Furthermore, combining the general type-II fuzzy logic sets with a modified harmony search algorithm technique adjust the controller to handle different uncertainties in complex power systems. The reference suggests a feasible method to enhance the robustness of system by applied a intelligent controller for the frequency control in microgrids. In , a model predictive control is exploited to solve the control problem of the blade pitch angles of the wind turbine and plug-in hybrid electric vehicles in LFC.

For the purpose of maintaining active power balance between generation and consumption, the traditional power systems principally regulate power of generation to trace the demand. Nonetheless, the reactive reserve needs to be increased to guarantee power balance. As the percentage of traditional generators reduces, it is challenging to ensure power balance by using the lacking active power reserve capacity . Thus, conventional regulating approach may not any more appropriate to maintain frequency stability due to dependence on the synchronous power supply. For the sake of

enhancing regulation capability, a exploration is necessary for a potential frequency regulation resource from other aspects. Coincidentally, demand response model offers an additional approach to maintain frequency stability by intervening the controllable load of demand side. With the improvement of living standard of inhabitants, the electricity consumption structure also changes accordingly. For example, the proportion of thermostatically controlled loads is rising inch by inch. Furthermore, thermostatically controlled loads are widely applied as participation in frequency control because of its economy and rapidity as a regulation resource. As a indispensable thermostatically controlled loads, inverter air conditioners (IACs) have no obvious influence on user experience when their state changes in a short time. Accordingly, IACs can be employed as alternative frequency regulation resource to compensate the frequency deviations arise in power grids, which reduce the operation pressure of generators. Recently, some relevant achievements are obtained. In , a coordinated control strategy is developed by utilizing IAC units and fixed frequency air-conditioning to participate secondary frequency regulation and primary frequency regulation, respectively, and a satisfied result for control performance is obtained. The paper propose a coordinated state-estimation method for air-conditioning loads to provide primary frequency regulation service, in which each air-conditioning unit is governed by a central coordinator and local controller. In order to regulate frequency effectively and serve customer better, the room thermal model and the IAC electrical model are deduced in and the frequency fluctuations are further diminished by a stochastic allocation method and a hybrid control strategy on this basis. As outlined, IAC is capable of implementing the improvement of frequency regulating ability, while none of aforementioned studies focus on the effect of frequency regulation for SMGs. The issue motivates this article.

From what has been discussed above, the delay-dependent stability issue is investigated by applying Lyapunov theory in SMG frequency regulation service with participation of IACs. In the following, the main contributions in this article are summarized:

(1) An LFC model is established to contain the multiple IAC aggregators and each aggregator has a time-varying delay characteristic under their underlying communication networks in IAC aggregators' domain. Furthermore, the system can be constructed a linear system with time-varying delay in state space, which contributes to obtain delay-dependent stability conditions by using Lyapunov-Krasovskii functional.

(2) In order to obtain less conservative stability criterion for the constructed system with single/multiple time-varying delays, the Wirtinger-based integral inequality and reciprocally convex combination lemma are employed to estimate the derivative of the LKF with a tighter bound. Then, the delay-dependent stability criterion is obtained in the form of linear matrix inequality.

(3) The effectiveness of the proposed approach is verified under three different configuration schemes, which illustrates the compensation effect of IACs on frequency imbalance. For robust performance in frequency regulation, the comparative analysis with different time delays is also carried out to confirm that the time delays adversely affect the frequency response and even causes it to diverge.

The rest part of this paper is organized as follows. The problem formulation and model construction are shown in Section 2. The main theoretical proof and analysis are presented in Section 3. Two examples are given to verify the effectiveness of the deduced criteria in Section 4. The conclusion is given in Section 5.

2. Problem formulation and model construction

In this section, the frequency control strategy that coordinates SMG and aggregated IACs is proposed and the structure of the studied SMG including IAC aggregators is described in Fig.1.

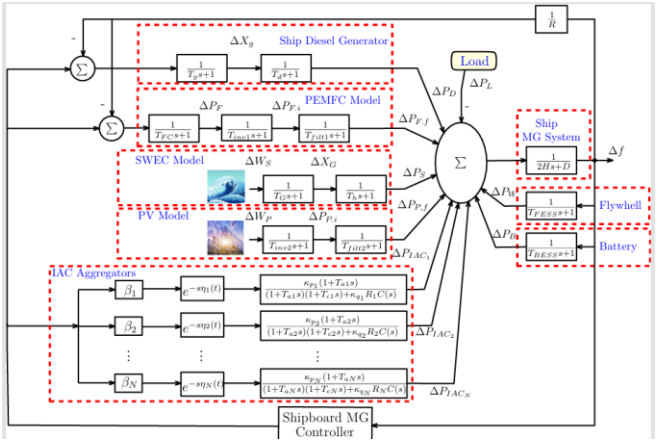

Figure 1. LFC scheme of a SMG with IAC aggregators

(1) IAC Aggregator

The power consumption of an IAC can supply flexible regulation power by adjusting the compressor operating frequency. The transfer function $\Theta\_i\ (s)$ of the ith IAC unit frequency response can be expressed as:

$$\Theta\_i\ (s) = (k\_p\ (1 + T\_ai\ s))/((1 + T\_ai\ s)(1 + T\_ci\ s) + k\_q\ R\_i\ C(s))$$

where $\llbracket T \rrbracket\ \_ci$ stands for the inertia time constant of the compressor. $T_ai = C_r\ R_i$b, $C_r$and R_i are the thermal capacity and thermal resistance of the room, respectively. k_q, k_p are coefficients of the cooling capacity and the power consumption, respectively. $C(s) = \chi + \varsigma/s$ represents the inbuilt tempreature controller, where χ, ς are proportional gain and integral gain , respectively.

(2) Shipboard MG Frequency Control Model Including IAC Aggregators

As depicted in Fig.2, the scheme of SMG is expressed in this paper, which consider the participant of IAC aggregators on the basis. Accordingly, the studied model including the IACs aggregators integrated into SMG is shown in Fig.2, and the state-space frequent response can be derived. In this framework, time delay occurs at the controller-IAC aggregator channel. Note that the time delay is different in each channel, and the delay in channel i is written as $\eta\_i\ (t), i = 1,2,\ldots,N$. In addition, N IAC aggregators hinge on the participation coefficients$\beta_1, \beta_2, \ldots, \beta_N$.

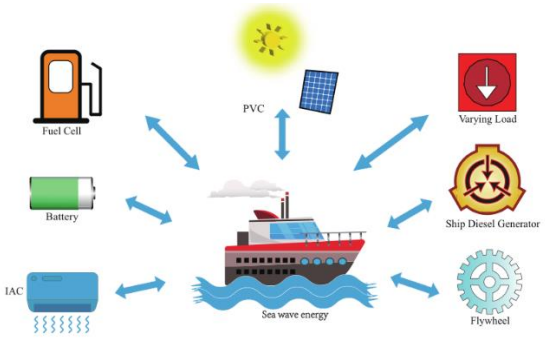

Figure 2. Components of a SMG

Now the state-space dynamic model of the SMG including N IAC aggregators with time delays can be constructed. According to the Fig.2, the following equations are obtained:

$$\begin{aligned}
\blacksquare(\Delta f^{\perp\cdot}\& &= 1/2H(\Delta P_D + \Delta P_(F,f) + \Delta P_S + \Delta P_(P,f) + \Delta P_B + \Delta P_W + \textstyle\sum_(i \\
&= 1)\hat{}N\equiv \Delta P_IACi - \Delta P_L - D\Delta f)@\Delta P^{\perp\cdot}_D\& \\
&= 1/T_d\ (\Delta X_g - \Delta P_D)@\Delta X^{\perp\cdot}_g\& \\
&= 1/T_g\ (\Delta U_S - \Delta X_g - 1/R\ \Delta f)@\Delta P^{\perp\cdot}_(F,f)\& \\
&= 1/T_filt1\ (\Delta P_(F,i) - \Delta P_(F,f))@\Delta P^{\perp\cdot}_(F,i)\& \\
&= 1/T_inv1\ (\Delta P_F - \Delta P_(F,i))@\Delta P^{\perp\cdot}_F\& \\
&= 1/T_FC\ (\Delta U_F - \Delta P_F - 1/R\ \Delta f)@\Delta P^{\perp\cdot}_S\& \\
&= 1/T_h\ (\Delta X_G - \Delta P_S)@\Delta X^{\perp\cdot}_G\& \\
&= 1/T_G\ (\Delta W_S - \Delta X_G)@\Delta P^{\perp\cdot}_(P,f)\& \\
&= 1/T_filt2\ (\Delta P_(P,i) - \Delta P_(P,f))@\Delta P^{\perp\cdot}_(P,i)\& \\
&= 1/T_inv2\ (\Delta W_P - \Delta P_(P,i))@\Delta P^{\perp\cdot}_B\& \\
&= 1/T_BESS\ (\Delta f - \Delta P_B)@\Delta P^{\perp\cdot}_W\& = 1/T_FESS\ (\Delta f - \Delta P_W))
\end{aligned}$$

Applying the inverse Laplace transform and defining corresponding state variables, it is obtained that:

$$\begin{aligned}
\blacksquare(x^{\perp\cdot}\ (t)\& &= Ax(t) + \textstyle\sum_(i = 1)\hat{}N\equiv C_i\ x(t - \eta_i\ (t)) + Bu(t) + F\omega(t)@y(t)\& \\
&= Ex(t)@x(t)\& = \phi(t), \forall t \\
&\in [-max\{\eta_1\ (t), \eta_2\ (t), \ldots, \eta_N\ (t)\}, 0])
\end{aligned}$$

where $\phi(t)$ is the system initial condition in the segment $[-max\{\eta\_1, \eta\_2 \ldots, \eta\_N\}, 0]$ and $x(t), \omega(t), A, B, C\_i, F$.

$$x(t) = col\{\Delta f\ \Delta P\_(D)\ \Delta X\_g\ \ \Delta P\_(F,f)\ \ \Delta P\_(F,i)\ \Delta P\_F\ \ \Delta P\_S\ \ \Delta X\_(G)\ \Delta P\_(P,f)\ \ \Delta P\_(P,i)\ \Delta P\_(B)\ \Delta P\_W\ \ \Delta P\_K1 \cdots \Delta P\_KN\}$$

$$\Delta P\_Ki = col\{\Delta P\_IACi\ \ \Delta P\_1i\ \ \Delta P\_2i\}(i = 1,2,\ldots,N)$$

$$\omega(t) = col\{\Delta P\_L\ \ \Delta W\_S\ \ \Delta W\_F\}$$

$$B = \mathbb{[}[\blacksquare(0\&0\&0\&0\&0\&1/T\_FC\ \&0\&0\&0\&0\&0\&0\&0\_(1\times 3)\&0\_(1\times 3)\&\cdots\&0\_(1\times 3)@0\&0\&1/T\_g\ \&0\&0\&0\&0\&0\&0\&0\&0\&0\&0\_(1\times 3)\&0\_(1\times 3)\&\cdots\&0\_(1\times 3))]\mathbb{]}\_(2\times(12+3N))\hat{}T$$

$$C\_i = Y\_i\ e\_(12+i), Y\_i = [(k\_pi\ \beta\_i)/T\_ci\ \ -(k\_pi\ \beta\_i)/(T\_ci\hat{}2)\ \ (k\_pi\ \beta\_i\ (T\_ai - T\_ci\ k\_qi\ R\_i\ \varepsilon))/(T\_ai\ T\_ci\hat{}2)\ ]\hat{}T, (i = 1,2,\ldots,N)$$

$$F = \mathbb{[}[\blacksquare(0\&0\&0\&0\&0\&0\&0\&0\&1/T\_inv2\ \&0\&0\&0\&0\_(1\times 3)\&0\_(1\times 3)\&\cdots\&0\_(1\times 3)@0\&0\&0\&0\&0\&0\&1/T\_G\ \&0\&0\&0\&0\&0\&0\_(1\times 3)\&0\_(1\times 3)\&\cdots\&0\_(1\times 3)@1/2H\&0\&0\&0\&0\&0\&0\&0\&0\&0\&0\&0\&0\_(1\times 3)\&0\_(1\times 3)\&\cdots\&0\_(1\times 3))]\mathbb{]}\_(3\times(12+3N))\hat{}T$$

$$E = \mathbb{[}[\blacksquare(1\&0\&0\&0\&0\&0\&0\&0\&0\&0\&0\&0\&0\_(1\times 3)\&0\_(1\times 3)\&\cdots\&0\_(1\times 3))]\mathbb{]}\_(1\times(12+3N))\hat{}T$$

$$A = [\blacksquare(A^{\perp\cdot}\&H@0\_(3N\times 12)\&A)]$$

$$\begin{aligned}
A^{\cdot} = [\blacksquare(&-D/2H\&1/2H\&0\&1/2H\&0\&0\&1/2H\&0\&1/2H\&0\&1/2H\&1/2H@0\& - 1/T_d\ \&1/T_d\ \&0\&0\&0\&0\&0\&0\&0\&0\&0@ - 1/(RT_g)\ \&0\& - 1/T_g\ \&0\&0\&0\&0\&0\&0\&0\&0\&0@0\&0\&0\& \\
&- 1/T_filt1\ \&1/T_filt1\ \&0\&0\&0\&0\&0\&0\&0\&0@0\&0\&0\&0\& - 1/T_inv1\ \&1/T_inv1\ \&0\&0\&0\&0\&0\&0@ - 1/(RT_FC)\&0\&0\&0\&0\& - 1/T_FC\ \&0\&0\&0\&0\&0\&0@0\&0\&0\&0\&0\&0\& \\
&- 1/T_h\ \&1/T_h\ \&0\&0\&0\&0\&0@0\&0\&0\&0\&0\&0\&0\&0\& - 1/T_G\ \&0\&0\&0\&0\&0@0\&0\&0\&0\&0\&0\&0\&0\& - 1/T_filt2\ \&1/T_filt2\ \&0\&0\&0@0\&0\&0\&0\&0\&0\&0\&0\&0\& \\
&- 1/T_inv2\ \&0\&0@1/T_BESS\ \&0\&0\&0\&0\&0\&0\&0\&0\&0\& - 1/T_BESS\ \&0@1/T_FESS\ \&0\&0\&0\&0\&0\&0\&0\&0\&0\& - 1/T_FESS\ )]
\end{aligned}$$

$$\mathbb{H} = [H\_1 \cdots H\_N], H\_i = [\blacksquare(1/2H\&0\&0\&0\&0\&0\&0\&0\&0\&0\&0\&0@0\&0\&0\&0\&0\&0\&0\&0\&0\&0\&0\&0\&0@0\&0\&0\&0\&0\&0\&0\&0\&0)]\hat{}T\ (i = 1,2,\ldots,N)$$

$$\begin{aligned}
A = [\blacksquare(&A_1\&0_(3\times 3)\&\cdots\&0_(3\times 3)@0_(3\times 3)\&A_2\&\cdots\&0_(3\times 3)@\vdots\ \&\vdots\ \&\ddots\ \&0_(3\times 3)@0_(3\times 3)\&0_(3\times 3)\&0_(3\times 3)\&A_N)], A_i \\
&= [\blacksquare(0\&1\&0@0\&0\&1@ - (k_qi\ R_i\ \eta_i)/(T_ai\ T_ci)\& - (1 + k_qi\ R_i\ \varepsilon_i)/(T_ai\ T_ci)\& - (T_ai + T_ci)/(T_ai\ T_ci))](i = 1,2,\ldots,N)
\end{aligned}$$

(3) Event-Triggered Control and Time-Delay Closed-Loop System Model

For the sake of saving limited network resources and avoiding communication channel congestion during the control process, the event-triggered control method is applied to maintain the SMG frequency stability . In the part, on basis of reference, an enhanced stretchy event-triggered mechanism (ESETM) is designed as follows:

$$r\hat{}T\ (t)G\_1\ r(t) - f((t\_k + j)l)x\hat{}T\ ((t\_k + j)l)G\_2\ x((t\_k + j)l) > \varrho((t\_k + j)l)$$

Where $l(l > 0)$ is the sampling detection period of sensor. $r(t) = x(t\_k\ l) - x((t\_k + j)l)$, $x((t_k + j)l)$is the current sampled state and $x(t\_k\ l)$ is the latest transmission data. G_1 and G_2 represent the positive definite symmetric matrices to be designed. In the actual control, if the state data satisfies the remote terminal unit will transmit the data to the controller to achieve the purpose of maintaining frequency stability. $\varrho((t\_k + j)l)$ is an internal dynamic variable satisfying:

$$\begin{aligned}
\varrho^{\cdot}((t_k + j)l) = &-\epsilon\varrho((t_k + j)l) + f((t_k + j)l)\ x\hat{}T\ ((t_k + j)l)\ G_2\ x((t_k + j)l) \\
&- r\hat{}T\ (t)\ G_1\ r(t)
\end{aligned}$$

in which ϵ is a positive scalar and $f(t) \in \mathbb{R}$ is an adaptive time-varying function to be designed. Moreover, $f(t)$ meets the following equation:

$$f^{\cdot}(t) = r^{\cdot}f(t)$$

Denoting $\daleth \triangleq r\hat{}T\ (t)\mathcal{G}\_1\ r(t)$, then the value of $(r\ )^{\cdot}$is designed in following formula:

$$\begin{aligned}
r^{\cdot} = \{\blacksquare(&-tan\partial \times (-\varpi\hat{}+) + r_1 \pm |\delta|, \&if\ > \varpi\hat{} + @0, \&if\ \in [\varpi\hat{}-, \varpi\hat{}+]@ \\
&- tan\partial \times (-\varpi\hat{}-) + r_2 \pm |\delta|, \&if\ < \varpi\hat{}-)\dashv
\end{aligned}$$

in which $r\_1 < 0$, $r\_2 < 0$, and $\varpi\hat{}-, \varpi\hat{}+ > 0$ are known constants and the parameter δ is a sufficiently small number satisfying: $\delta > 0$. Moreover, adopting $\partial(\partial \in [0, \pi/2))$to describe the degree of change in $\bar{r}$ under the change of $\daleth$.

Assumption 1. The function $f(t)$ is a bounded function and $0 \le f\_l \le f(t) \le f\_u$, besides the initial value of $f(t)$ satisfies $f(0) \in [0,1)$.

Remark 1. Compared with the triggered scheme of , the enhanced adaptive function $f(t)$ is introduced in the proposed ESETM. This enhanced adaptive function has a more larger variable range. To be specific, when the deviation between the latest triggered system state and the current sampled system state is too large, the enhanced adaptive function plays a significant role in the process of optimizing network resources utilization. Namely, the smaller (larger) $f(t)$ is, the released rate of sampled state is more (less).

Remark 2. The ESETM is more general compared with some existing event-triggered mechanisms. If $\Psi\_1 = \Psi\_2$ and $\mathcal{F}(t) = 0$, then it can be reduced to the ETM applied in [10]. If $\Psi\_1 = \Psi\_2$, $\mathcal{F}(t) = 0$ and$r^{\cdot} \equiv 0$, then it can be simplified as the ETM proposed in and [12]. If $\Psi\_1 = \Psi\_2$ and $r^{\cdot} \equiv 0$, then it can be converted to the ETM employed in and [14]. If $\mathbb{[}\ \Psi\mathbb{]}\ \_1 = \Psi\_2 = I\_n$ and $\mathcal{F}(t) = 0$, then it can be changed to the similar expression of the ETM utilized in . Thus, the ESETM in this article is more flexible and comprehensive.

Without loss of generality, based on the event-triggered mechanism, the controller can be re-described as:

$$u(t) = Kx(t\_k\ l)$$

Denoting $\aleph\_k = t\_(k + 1) - t\_k - 1$, then the interval $[t\_k\ l, t\_(k + 1)\ l)$ can be represented as:

$$[t\_k\ l, t\_(k+1)\ l) = \cup\_(j=0)\hat{}(\aleph\_k)\ \Gamma\_j\hat{}(t\_k)$$

where $\Gamma\_j\hat{}(t\_k) = [t\_k\ l + jl, t\_k\ l + (j+1)l), j = 0,1,\ldots,\aleph\_k$. Applying the definition $\sigma(t) = t - (t\_k + j)l$, One can understand that $x(t_k\ l + jl) = x(t - \sigma(t))andx(t_k\ l) = r(t) + x(t - \sigma(t))$. Then, on the basis of (2.11), the inequality can be deduced:

$$r\hat{}T\ (t)\ G\_1\ r(t) - f(t-\sigma(t))\ x\hat{}T\ (t-\sigma(t))\ G\_2\ x(t-\sigma(t)) > \varrho(t-\sigma(t))$$

Furthermore, for $[t\_k\ l, t\_(k+1)\ l)$, the controller is re-expressed as:

$$u(t) = K[x(t-\sigma(t)) + r(t)]$$

Substituting the following time-delay closed-loop system model:

$$\dot{x}(t) = Ax(t) + \sum\_(i=1)\hat{}N\ C\_i\ x(t-\eta\_i(t)) + BK[x(t-\sigma(t)) + r(t)] + F\omega(t)$$

Definition 1. For any initial condition $x(0)$, the system with $\omega(t) = 0$ is said to be asymptoticall stable if the following equation holds:

$$\mathbb{lim}\_(t\to\infty)\ \| x(t) \| = 0$$

Definition 2. The system is referred to H_∞ have performance with disturbance attenuation level $\epsilon > 0$, if the following conditions holds:

(i)The system are asymptotically stable when the exogenous disturbance $\omega(t) = 0$.

(ii)The system has weighted L_2-gain from exogenous disturbance $\omega(t) \neq 0$ to the controlled output $y(t)$ under the zero initial condition, i.e.

$$\int\_0\hat{}\infty\ y\hat{}T\ (t) y(t) dt \le \epsilon\hat{}2 \int\_0\hat{}\infty\ \omega\hat{}T\ (t)\omega(t) dt$$

Lemma 1. For a symmetric matrix $T > 0$, any differentiable function e in $[\alpha,\beta] \to \mathbb{R}\hat{}n$, the following inequality holds:

$$\int\_\alpha\hat{}\beta\ \dot{e}\hat{}T\ (\omega) T \dot{e}(\omega) d\omega \ge 1/(\beta-\alpha)\ [\blacksquare(e(\beta) - e(\alpha)@\aleph(\alpha,\beta))]\hat{}T\ T[\blacksquare(e(\beta) - e(\alpha)@\aleph(\alpha,\beta))]$$

where $T = diag\{T, 3T\}, \aleph(\alpha,\beta) = e(\beta) + e(\alpha) - 2/(\beta-\alpha)\int\_\alpha\hat{}\beta\ e(\omega) d\omega.$

Lemma 2. . If $0 \le \eta(t) \le \bar{\eta}$, for any matrices $H \in \mathcal{R}\hat{}(n\times n)$ and $L \in \mathcal{R}\hat{}(n\times n)$ that satisfy $[\blacksquare(H\&L@\star\ \&H)] > 0$, then the following inequality holds:

$$-\bar{\eta}\int\_(t-\bar{\eta})\hat{}t\ \dot{x}\hat{}T\ (s) H \dot{x}(s) ds \le [\blacksquare(x(t)@x(t-\eta(t))@x(t-\bar{\eta}))]\hat{}T\ [\blacksquare(-H\&H - L\&L@\star\ \& - 2H + L\hat{}T + L\&H - L@\star\ \&\star\ \& - H)][\blacksquare(x(t)@x(t-\eta(t))@x(t-\bar{\eta}))]$$

3. Main results

The system with a single time-varying delay is considered:

$$\dot{x}(t) = Ax(t) + Cx(t-\eta(t)) + BK[x(t-\sigma(t)) + r(t)] + F\omega(t)$$
$$y(t) = Ex(t)$$
$$x(t) = \varphi(t), \forall t \in [\bar{\eta}, 0]$$

where $x(t)$ is the system state vector, $\eta(t)$ is a time-varying differentiable function and $\bar{\eta}$ is the upper bound of $\eta(t)$. The following inequalities holds:

$$0 \le \eta(t) \le \bar{\eta}, \eta\_L \le \dot{\eta}(t) \le \eta\_U < 1$$

where η_L, $\eta_U$and $\bar{\eta}$ are known constants.

Theorem. For given scalars $\eta\_L, \eta\_U, \bar{\eta}$, the system is asymptotically stable if there exist symmetric positive definite matrices $Q \in R^{3n\times 3n}, \mathcal{R}\_1 \in R^{n\times n}, \mathcal{R}\_2 \in R^{n\times n}, S \in R^{2n\times 2n}, T \in R^{n\times n}$ such that:

$$\daleth\_(\eta(t),\dot{\eta}(t)) < 0$$

$$\begin{bmatrix} \Theta^1\_{(\dot{\eta}(t))} & U \\ \star & \Theta^2\_{(\dot{\eta}(t))} \end{bmatrix} > 0$$

$$\begin{bmatrix} T & L \\ \star & T \end{bmatrix} > 0$$

Where

$$\daleth\_{(\eta(t),\dot{\eta}(t))} = \daleth\_{1(\eta(t))} + \daleth\_{2(\eta(t),\dot{\eta}(t))} + \daleth\_{3(\eta(t),\dot{\eta}(t))} + \daleth\_4 - \Pi\_{(\eta(t))} + \Psi,$$
$$\daleth\_{1(\eta(t))} = He\{[\lambda\_1\lambda\_5\lambda\_6]^T \mathcal{Q}[\lambda\_4\lambda\_1 - (1-\dot{\eta}(t))\lambda\_2(1-\dot{\eta}(t))\lambda\_2 - \lambda\_3]\},$$
$$\daleth\_{2(\eta(t),\dot{\eta}(t))} = \bar{\eta}\eta(t)(\lambda\_1^T\mathcal{R}\_1\lambda\_1 - (1-\dot{\eta}(t))\lambda\_2^T\mathcal{R}\_1\lambda\_2) - \bar{\eta}He\{\lambda\_5^T\mathcal{R}\_1(\lambda\_1 - (1-\dot{\eta}(t))\lambda\_2)\}$$
$$-3\bar{\eta}He\{(\lambda\_5 - 2\lambda\_9)^T\mathcal{R}\_1(\lambda\_1 - (1-\dot{\eta}(t))\lambda\_2 + 2\dot{\eta}(t)\lambda\_{11} - 2\lambda\_1 + 2(1-\dot{\eta}(t))\lambda\_7)\},$$
$$\daleth\_{3(\eta(t),\dot{\eta}(t))} = (\bar{\eta} - \eta(t))\eta(t)((1-\dot{\eta}(t))\lambda\_2^T\mathcal{R}\_2\lambda\_2 - \lambda\_3^T\mathcal{R}\_2\lambda\_3) - \bar{\eta}He\{\lambda\_6^T\mathcal{R}\_2((1-\dot{\eta}(t))\lambda\_2 - \lambda\_3)\}$$
$$-3\bar{\eta}He\{(\lambda\_6 - 2\lambda\_{12})^T\mathcal{R}\_2((1-\dot{\eta}(t))\lambda\_2 - \lambda\_3 - 2\dot{\eta}(t)\lambda\_{12} - 2(1-\dot{\eta}(t))\lambda\_2 + 2\lambda\_8)\},$$
$$\daleth\_4 = \bar{\eta}^2[\lambda\_4\lambda\_1]^T\mathcal{S}[\lambda\_4\lambda\_1] + \bar{\eta}[\lambda\_1\lambda\_2\lambda\_3]^T diag\{J\_1, J\_2 - J\_1, J\_2\}[\lambda\_1\lambda\_2\lambda\_3],$$
$$\Pi\_{(\eta(t))} = [\Pi\_1 \ \Pi\_2]^T \begin{bmatrix} \Theta^1\_{(\eta(t))} & U \\ \star & \Theta^2\_{(\eta(t))} \end{bmatrix} [\Pi\_1 \ \Pi\_2],$$
$$\Pi\_1 = col\{\lambda\_1 - \lambda\_2, \lambda\_5, \lambda\_1 - \lambda\_2 - 2\lambda\_5, \lambda\_5 - 2\lambda\_9\},$$
$$\Pi\_2 = col\{\lambda\_2 - \lambda\_3, \lambda\_6, \lambda\_2 - \lambda\_3 - 2\lambda\_6, \lambda\_6 - 2\lambda\_{10}\}, \Theta\_i = diag\{\mathcal{S}\_i, 3\mathcal{S}\_i\}(i = 1,2)$$
$$\Psi = \bar{\eta}^2\lambda\_4^T\mathcal{T}\lambda\_4 - \lambda\_{13}^T\mathcal{W}\lambda\_{13} + \bar{\lambda}^T\mathbf{T}\bar{\lambda} - He\{\lambda\_{14}^T\mathcal{G}\_1\lambda\_{14}\} + f\_u He\{\lambda\_{13}^T\mathcal{G}\_2\lambda\_{13}\}$$
$$+He\{(n\_1\lambda\_4^T N\_1 + n\_2\lambda\_1^T N\_2)(-\lambda\_4 + \tilde{A}\_1\lambda\_1 + \tilde{A}\_2\lambda\_2 + \tilde{B}\_1 K\lambda\_{13} + \tilde{B}\_1 K\lambda\_{14} + F\lambda\_{15})\},$$
$$\bar{\lambda} = col\{\lambda\_1, \lambda\_2, \lambda\_3\}, \mathbf{T} = \begin{bmatrix} -\mathcal{T} & \mathcal{T} - \mathcal{L} & \mathcal{L} \\ \star & -2\mathcal{T} + \mathcal{L}^T + \mathcal{L} & \mathcal{T} - \mathcal{L} \\ \star & \star & -\mathcal{T} \end{bmatrix}$$

Proof. The following LKF candidate is applied for the system:

$$V(t) = \sum\_{i=1}^{5} V\_i(t) + \varrho\big(t - \sigma(t)\big), t \in \Gamma\_j^{t\_k}$$

where

$$V\_1(t) = \chi^T(t)\mathcal{Q}\chi(t), \chi(t) = col\{x(t), \int\_{t-\eta(t)}^{t} x(s)ds, \int\_{t-\bar{\eta}}^{t-\eta(t)} x(s)ds\},$$
$$V\_2(t) = \bar{\eta}\eta(t)\int\_{t-\eta(t)}^{t} x^T(s)\mathcal{R}\_1 x(s)ds - \bar{\eta}(\int\_{t-\eta(t)}^{t} x(s)ds)^T\mathcal{R}\_1(\diamondsuit)$$
$$-3\bar{\eta}(\int\_{t-\eta(t)}^{t} x(s)ds - \frac{2}{\eta(t)}\int\_{t-\eta(t)}^{t}\int\_{s}^{t} x(u)duds)^T\mathcal{R}\_1(\diamondsuit),$$
$$V\_3(t) = \bar{\eta}(\bar{\eta} - \eta(t))\int\_{t-\bar{\eta}}^{t-\eta(t)} x^T(s)\mathcal{R}\_2 x(s)ds - \bar{\eta}(\int\_{t-\bar{\eta}}^{t-\eta(t)} x(s)ds)^T\mathcal{R}\_2(\diamondsuit)$$
$$-3\bar{\eta}(\int\_{t-\bar{\eta}}^{t-\eta(t)} x(s)ds - \frac{2}{\bar{\eta} - \eta(t)}\int\_{t-\bar{\eta}}^{t-\eta(t)}\int\_{s}^{t} x(u)duds)^T\mathcal{R}\_2(\diamondsuit),$$
$$V\_4(t) = \bar{\eta}\int\_{t-\bar{\eta}}^{t}\int\_{s}^{t} \zeta^T(u)\mathcal{S}\zeta(u)duds, \zeta(t) = col\{\dot{x}(t), x(t)\},$$
$$V\_5(t) = \bar{\eta}\int\_{t-\bar{\eta}}^{t}\int\_{s}^{t} \dot{x}^T(u)\mathcal{T}\dot{x}(u)duds,$$
$$V\_6(t) = (l-t)x^T(t-\sigma(t))\mathcal{W}x(t-\sigma(t)).$$

The derivative of $V(t)$ along the trajectory of system are as follow:

$$\dot{V}\_1(t) = 2\chi^T(t)\mathcal{Q}\dot{\chi}(t) = \mathfrak{f}^T(t)\daleth\_{1(\eta(t))}\mathfrak{f}(t)$$
$$\dot{V}\_2(t) = \dot{\bar{\eta}}\eta(t)\int\_{t-\eta(t)}^{t} x^T(s)\mathcal{R}\_1 x(s)ds + \bar{\eta}\dot{\eta}(t)(x^T(t)\mathcal{R}\_1 x(t) - (1-\dot{\eta}(t))x^T(t-\eta(t))\mathcal{R}\_1 x(t-\eta(t)))$$
$$-2\bar{\eta}(\int\_{t-\eta(t)}^{t} x(s)ds)^T\mathcal{R}\_1(\dot{\diamondsuit}) - 6\bar{\eta}(\int\_{t-\eta(t)}^{t} x(s)ds - \frac{2}{\eta(t)}\int\_{t-\eta(t)}^{t}\int\_{s}^{t} x(u)duds)^T\mathcal{R}\_1(\dot{\diamondsuit})$$
$$= \dot{\bar{\eta}}\eta(t)\int\_{t-\eta(t)}^{t} x^T(s)\mathcal{R}\_1 x(s)ds + \mathfrak{f}^T(t)\daleth\_{2(\eta(t),\dot{\eta}(t))}\mathfrak{f}(t)$$
$$\dot{V}\_3(t) = -\dot{\bar{\eta}}\eta(t)\int\_{t-\bar{\eta}}^{t-\eta(t)} x^T(s)\mathcal{R}\_2 x(s)ds + (\bar{\eta} - \eta(t))\dot{\eta}(t)((1-\dot{\eta}(t))x^T(t-\eta(t))\mathcal{R}\_2 x(t-\eta(t)) - x^T(t-\bar{\eta})\mathcal{R}\_2 x(t-\bar{\eta}))$$
$$-2\bar{\eta}(\int\_{t-\bar{\eta}}^{t-\eta(t)} x(s)ds)^T\mathcal{R}\_2(\dot{\diamondsuit}) - 6\bar{\eta}(\int\_{t-\bar{\eta}}^{t-\eta(t)} x(s)ds - \frac{2}{\bar{\eta} - \eta(t)}\int\_{t-\bar{\eta}}^{t-\eta(t)}\int\_{s}^{t} x(u)duds)^T\mathcal{R}\_2(\dot{\diamondsuit})$$
$$= -\dot{\bar{\eta}}\eta(t)\int\_{t-\bar{\eta}}^{t-\eta(t)} x^T(s)\mathcal{R}\_2 x(s)ds + \mathfrak{f}^T(t)\daleth\_{3(\eta(t),\dot{\eta}(t))}\mathfrak{f}(t)$$
$$\dot{V}\_4(t) = \bar{\eta}^2\zeta^T(t)\mathcal{S}\zeta(t) - \bar{\eta}\int\_{t-\bar{\eta}}^{t} \zeta^T(s)\mathcal{S}\zeta(s)ds$$
$$\dot{V}\_5(t) = \bar{\eta}^2\dot{x}^T(t)\mathcal{T}\dot{x}(t) - \bar{\eta}\int\_{t-\bar{\eta}}^{t} \dot{x}^T(s)\mathcal{T}\dot{x}(s)ds$$
$$\dot{V}\_6(t) = -x^T(t-\sigma(t))Wx(t-\sigma(t))$$

where $\mathfrak{f}(t) = \{\mathfrak{f}\_1(t), \mathfrak{f}\_2(t), \mathfrak{f}\_3(t), \mathfrak{f}\_4(t)\}$,

$$\mathfrak{f}\_1(t) = \{x(t), x(t-\eta(t)), x(t-\bar{\eta}), \dot{x}(t)\}$$
$$\mathfrak{f}\_2(t) = \{\int\_{t-\eta(t)}^{t} x(s)ds, \int\_{t-\bar{\eta}}^{t-\eta(t)} x(s)ds, \frac{1}{\eta(t)}\int\_{t-\eta(t)}^{t} x(s)ds, \frac{1}{\bar{\eta} - \eta(t)}\int\_{t-\bar{\eta}}^{t-\eta(t)} x(s)ds\}$$
$$\mathfrak{f}\_3(t) = \{\frac{1}{\eta(t)}\int\_{t-\eta(t)}^{t}\int\_{s}^{t} x(u)duds, \frac{1}{\bar{\eta} - \eta(t)}\int\_{t-\bar{\eta}}^{t-\eta(t)}\int\_{s}^{t} x(u)duds, \frac{1}{\eta(t)^2}\int\_{t-\eta(t)}^{t}\int\_{s}^{t} x(u)duds, \frac{1}{(\bar{\eta} - \eta_t)^2}\int\_{t-\bar{\eta}}^{t-\eta(t)}\int\_{s}^{t} x$$
$$\mathfrak{f}\_4(t) = \{x(t-\sigma(t)), r(t), \omega(t)\}$$

According to the Newton-Leibniz formula, the following zero equation is considered for the symmetric positive definite matrices J_1, J_2:

$$0 = \bar{\eta}\left[x^T(t)x^T\left(t-\eta(t)\right)\right]diag\{J_1,J_1\}(\Diamond) - 2\bar{\eta}\int_{t-\eta(t)}^{t} x^T(s)J_1\dot{x}(s)ds + \bar{\eta}\left[x^T\left(t-\eta(t)\right)x^T(t - \bar{\eta})\right]diag\{J_2,J_2\}(\Diamond) - 2\bar{\eta}\int_{t-\bar{\eta}}^{t-\eta(t)} x^T(s)J_2\dot{x}(s)ds$$

Denote

$$\mathfrak{I} \triangleq \mathfrak{f}^T(t)\Xi\mathfrak{f}(t) - \bar{\eta}\int_{t-\eta(t)}^{t} \zeta^T(s)\mathcal{S}_1\zeta(s)ds - \bar{\eta}\int_{t-\bar{\eta}}^{t-\eta(t)} \zeta^T(s)\mathcal{S}_2\zeta(s)ds$$

Subsequently, the integral terms are bounded by employing **Lemma 1**:

$$-\bar{\eta}\int_{t-\eta(t)}^{t}\zeta^T(s)S_1\zeta(s)ds \le -\frac{\bar{\eta}}{\eta(t)}\left(\int_{t-\eta(t)}^{t}\zeta(s)ds\right)^T S_1(\Diamond) - \frac{3\bar{\eta}}{\eta(t)}\left(\int_{t-\eta(t)}^{t}\zeta(s)ds - \frac{2}{\eta(t)}\int_{t-\eta(t)}^{t}\int_{s}^{t}\zeta(u)duds\right)^T S_1(\Diamond) = -\frac{\bar{\eta}}{\eta(t)}\ ^T(t)\Pi_1^T\Theta_1\Pi_1(t)$$

and

$$-\bar{\eta}\int_{t-\bar{\eta}}^{t-\eta(t)}\zeta^T(s)S_2\zeta(s)ds \le -\frac{\bar{\eta}}{\bar{\eta}-\eta(t)}\left(\int_{t-\bar{\eta}}^{t-\eta(t)}\zeta(s)ds\right)^T S_1(\Diamond) - \frac{3\bar{\eta}}{\bar{\eta}-\eta(t)}\left(\int_{t-\bar{\eta}}^{t-\eta(t)}\zeta(s)ds - \frac{2}{\bar{\eta}-\eta(t)}\int_{t-\bar{\eta}}^{t-\eta(t)}\int_{s}^{t}\zeta(u)duds\right)^T S_2(\Diamond) = -\frac{\bar{\eta}}{\bar{\eta}-\eta(t)}\ ^T(t)\Pi_2^T\Theta_2\Pi_2(t)$$

where

$$\Pi_1 = col\{\lambda_1-\lambda_2, \lambda_5, \lambda_1-\lambda_2-2\lambda_5, \lambda_5-2\lambda_9\}$$
$$\Pi_2 = col\{\lambda_2-\lambda_3, \lambda_6, \lambda_2-\lambda_3-2\lambda_6, \lambda_6-2\lambda_{10}\}$$
$$\Theta_i = diag\{S_i, 3S_i\}$$

Then, a upper bound of $\mathfrak{I}$ can be calculated as:

$$\mathfrak{I} \le \mathfrak{f}^T(t)(\mathfrak{I}_4 - (\frac{\overline{\eta}}{\eta(t)}\Pi_1^T\Theta_1\Pi_1 + \frac{\overline{\eta}}{\overline{\eta}-\eta(t)}\Pi_2^T\Theta_2\Pi_2))\mathfrak{f}(t)$$

By applying Lemma 2, it implies that:

$$\mathfrak{I} \le \mathfrak{f}^T(t)(\mathfrak{I}_4 - (\Pi_1^T\Theta_1\Pi_1 + \Pi_2^T\Theta_2\Pi_2 + 2\Pi_1^T U\Pi_2))\mathfrak{f}(t) = \mathfrak{f}^T(t)(\mathfrak{I}_4 - \Pi)\mathfrak{f}(t)$$

Given scalars n_1, n_2 and appropriate dimensions matrices N_1, N_2, it is easy to obtain that:

$$0 = 2[n_1x(t)N_1 + n_2x(t)N_2][-\dot{x}(t) + Ax(t) + Cx(t-\eta(t)) + BK(x(t-\sigma(t)) + r(t)) + F\omega(t)]$$

According to the above mathematical operations, taking the event-triggered mechanism into account, then the following inequality can be derived:

$$\dot{\mathbf{V}}(t) \le \mathfrak{f}^T(t)(\mathfrak{I}_{1_{(\eta(t))}} + \mathfrak{I}_{2_{(\eta(t),\eta(t))}} + \mathfrak{I}_{3_{(\eta(t),\eta(t))}} + \mathfrak{I}_4 - \Pi)\mathfrak{f}(t) + \bar{\eta}^2\dot{x}^T(t)\mathcal{T}\dot{x}(t) - x^T(t-\sigma(t))Wx(t-\sigma(t)) + [x(t-\eta(t))]^T\begin{bmatrix} x(t) & -\mathcal{T} & \mathcal{T}-\mathcal{L} & \mathcal{L} & x(t) \\ \star & -2\mathcal{T}+\mathcal{L}^T+\mathcal{L} & \mathcal{T}-\mathcal{L} & [x(t-\eta(t))] & \\ x(t-\bar{\eta}) & \star & \star & -\mathcal{T} & x(t-\bar{\eta}) \end{bmatrix} + 2[n_1\dot{x}(t)N_1 + n_2x(t)N_2][-\dot{x}(t) + Ax(t) + Cx(t-\eta(t)) + BK(x(t-\sigma(t)) + r(t)) + F\omega(t)] + \varrho(t-\sigma(t)) - r^T(t)\mathcal{G}_1r(t) + f(t-\sigma(t))x^T(t-\sigma(t))\mathcal{G}_2x(t-\sigma(t)) + \varrho(t-\sigma(t)) \le \mathfrak{f}^T(t)\mathfrak{I}_{(\eta(t),\eta(t))}\mathfrak{f}(t) + (1-\delta)\varrho(t-\sigma(t))$$

4. Numerical examples

In this section, some simulation examples are given to confirm the effectiveness and superiority of developed tactic. The following is a simulated procedure for this study:

Firstly, in order to highlight the role of IAC aggregators more obviously in SMG frequency regulation, the load, solar power and sea wave power are all set to step signals and are connected to SMG at different instants, respectively, which cause different levels of frequency deviation. Then the effect of IAC aggregators can be qualitatively analysed by the obtained frequency fluctuation response and further acquire the optimized participation ratios. On this basis, considering plugging practical signal of the load, solar power and sea wave power into SMG and quantitatively analysing the influence of delay on frequency fluctuation. The simulation is based on the parameters in the Table.1 and Table.2.

Table 1. Parameters of SMG

Parameters	H	D	T_{FC}	T_g	T_{inv1}	T_{inv2}	T_G
Values	0.2	0.012	0.26	1	0.04	4	0.5
Parameters	T_d	T_{filt1}	T_{filt2}	T_h	T_{BESS}	T_{FESS}	
Values	2	0.004	0.5	4	0.1	0.1	

Table 2. Parameters of IAC aggregators

Parameters	χ	ς	C_r	R_i	k_p	k_q	T_{ci}
Values	0.52	0.032	60.55	3.191	0.016	0.035	0.02
Units	$Hz/^\circ C$	$Hz/(^\circ C\ s)$	$kJ/^\circ C^\circ$	C/kW	Hz	kW/Hz	s

5. Frequency deviation under step signals

In the simulation, three groups of IAC aggregators are configured in SMG. The contribution of the generator and IAC aggregators is compared and without discussing the influence of time delay. Since the IAC aggregator parameters of each group are different, there are three configuration schemes:

Scheme I. No IAC aggregator configuration: None of the three groups IAC aggregators are configured in SMG.

Scheme II. Equivalent IAC aggregator configuration: The participation coefficient of IAC aggregators in each group is equal.

Scheme III. Optimized IAC aggregator configuration: Based on the parameter difference of the three groups of IAC aggregators and the adjustment of the numerical optimization algorithm, when the obtained frequency fluctuation convergence effect is optimal, the participation coefficient allocation of the three groups of IAC aggregators is the optimized IAC aggregator configuration.

Furthermore, the frequency fluctuation response under three different configuration schemes are investigated. As shown in Fig.3, the load, sea wave power and solar power are respectively connected to SMG at $t=5s, 35s, 65s$, and the corresponding frequency fluctuation response for various participation coefficients under different penetration levels of RESs are illustrated in Fig.4.

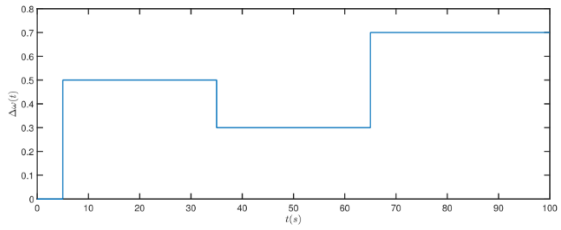

Figure 3. The disturbance at different instants

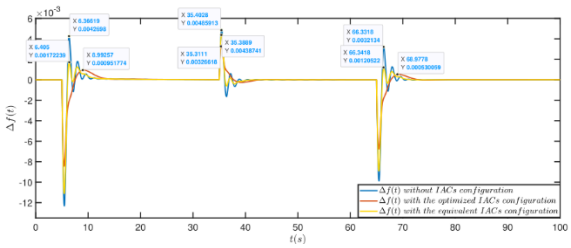

Figure 4. The frequency response with different schemes

In Fig.4, there are jumping change in frequency due to the infiltration of load, sea wave power and solar power at t= 5s, 35s, 65s, respectively. The frequency fluctuations have different dynamic response under different IAC aggregator configurations. Under the above three IAC aggregator configuration schemes I, II, III, the overshoot of the frequency response curve decreases successively. It can be obviously concluded that IAC aggregators has a favorable influence on frequency regulation. Furthermore, the regulation effects on frequency are also different with the different participation coefficients of IAC aggregator.

In order to quantitatively evaluate the dynamic performance of the system during the transient response period under three configuration schemes, the performance indices are utilized to quantify the dynamic performance, including the integral of the absolute value of the error (ITAE), the integral of time multiplied square error (ITSE), the integral of time multiplied absolute value of the error (IAE), the integral of square error (ISE). Then, the performance indices used are defined as follows:

$$ITAE = \int_0^{T_{sim}} t|\Delta f|dt, ITSE = \int_0^{T_{sim}} t(\Delta f)^2 dt, IAE = \int_0^{T_{sim}} |\Delta f|dt, ISE = \int_0^{T_{sim}} (\Delta f)^2 dt.$$

where T_{sim} represents the simulation duration and sets it to \$100s\$ in this simulation. The performance indices are listed in Table.3 by simulation, which reveals scheme III having the smaller values performs the better dynamic response without considering the influence of time delay.

Table 3. Performance indicators for SMG under three configuration schemes

Scheme	ITAE	ITSE	IAE	ISE
Scheme I	13.0646	0.0740	0.4297	0.0027
Scheme II	10.5841	0.0436	0.3443	0.0016
Scheme III	8.7638	0.0218	0.2649	0.0010

6. Frequency deviation under practical signals

The signals of the load, solar power and sea wave power applied on SMG are considered in real situations. In this paper, the load signal is step signal. The real data of the SWE fluctuation and solar radiation are considered, which are provided in Fig.5. Fig.6 shows the frequency response of the simulated closed-loop SMG system under three different configuration schemes when the practical signals is connected. As shown in Fig.6, the participation of IAC aggregators provides a lower amplitude of the frequency deviations than those in. Similarly, the simulation duration is also set as 100s and the performance indices are listed in Table.4 by simulation, which reveals scheme III having the smaller values performs the better dynamic response without considering the influence of time delay.

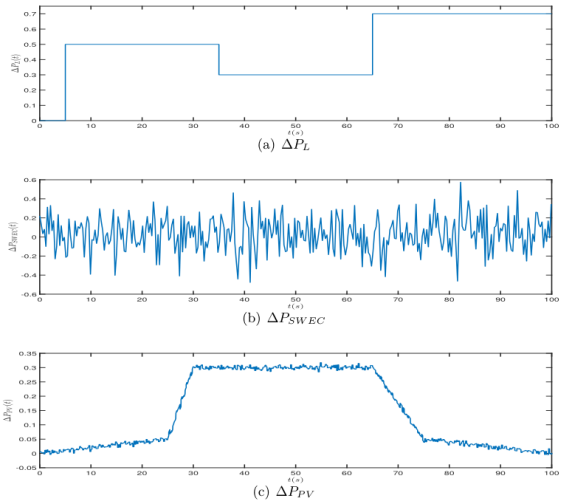

Figure 5. Power fluctuations

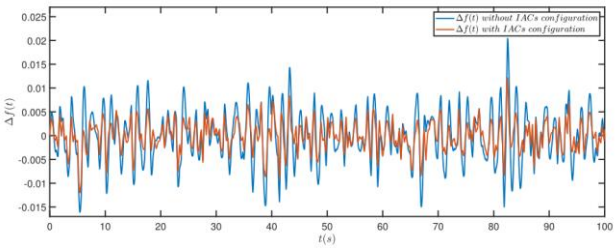

Figure 6. The frequency response with different schemes

Following the process in the previous subsection, the effect of time delay on the frequency response will be analysed on the basis of scheme III. The two groups of time delays are still set as Table 4. The frequency response of SMG under the circumstance of considering time delays are shown in Fig.7. As can be seen from Fig.7, when time delay is not taken into account, the frequency response will fluctuate with irregular margin under the intervention of RESs. When the delay is the Group 1, the amplitude of the frequency response is larger than it would be without the time delay; when the delay is the Group 2, the frequency response is also unstable and even divergent. Fig.8 is drawn to visually observe the impact of time delay on frequency response performance indicators.

Table 4. Performance indicators for SMG under three configuration schemes

Scheme	ITAE	ITSE	IAE	ISE
Scheme I	873.3782	5.9964	17.8107	0.1215
Scheme II	10.5841	0.0436	0.3443	0.0016
Scheme III	502.4777	1.9009	10.2003	0.0398

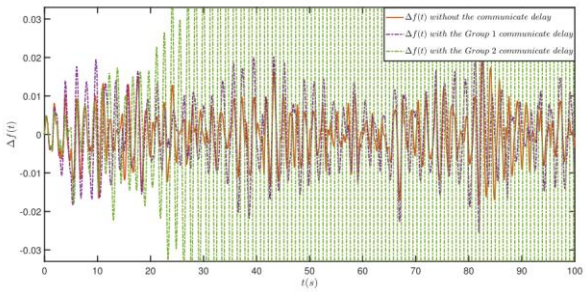

Figure 7. The frequency response with different delays

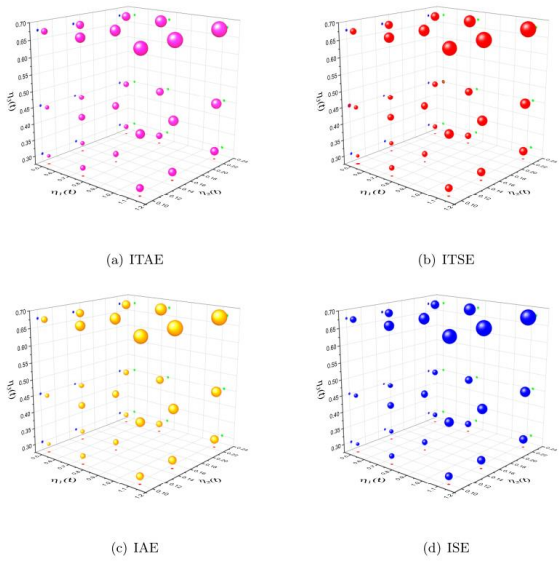

Figure 8. The performance indices with different delays

In conclusion, the existence of communication delay affects the frequency response whether the step signals or the practical signals is connected to SMG. And participate of IAC can play a better effect by providing a part of the frequency support in frequency regulation.

7. Conclusion

In order to reduce environmental pollution and improve the sustainable development of the SMG. This work develops a demand response scheme to deal with the challenges brought by the randomness and intermittency of sustainable energy in power system. The proposed ESETM is exploited and can realize a trade-off between the life of the control equipments and system performance. By choosing appropriate LKF candidate and some delay-dependent techniques, the sufficient conditions of the established closed-loop system can achieve stability are deduced and the controller is also designed to guarantee frequency stability of the SMG in Theorem when involved only single time-varying delays (N = 1). Finally, the simulation experiments show that the proposed method can ensure the stable operation of the SMG with the large penetration of RESs by providing frequency reserve of IAC aggregators.

Acknowledgements

This work is partially supported by 2023 the Fundamental Research Funds for the Central Universities-provincial and ministerial platform construction special projects (2023NYXXS009).

References

[1] E. Skjong, R. Volden, E. Rødskar, M. Molinas, T. A. Johansen, J. Cunningham, Past, present, and future challenges of the marine vessels electrical power system, IEEE Transactions on Transportation Electrification 2 (4) (2016) 522–537.

[2] E. Skjong, E. Rdskar, M. Molinas, T. A. Johansen, J. Cunningham, The marine vessels electrical power system: From its birth to present day, Proceedings of the IEEE 103 (12) (2015) 2410–2424.

[3] T. J. McCoy, Electric ships past, present, and future [technology leaders], IEEE Electrification Magazine 3 (2) (2015) 4–11.

[4] M. Tadros, M. Ventura, C. G. Soares, Review of current regulations, available technologies, and future trends in the green shipping industry, Ocean Engineering 280 (2023) 114670.

[5] G. F. Reed, B. M. Grainger, A. R. Sparacino, Z.-H. Mao, Ship to grid: Medium-voltage dc concepts in theory and practice, IEEE Power and Energy Magazine 10 (6) (2012) 70–79.

[6] R. E. Hebner, F. M. Uriarte, A. Kwasinski, A. L. Gattozzi, H. B. Estes, A. Anwar, P. Cairoli, R. A. Dougal, X. Feng, H.-M. Chou, et al., Technical cross-fertilization between terrestrial microgrids and ship power systems, Journal of Modern Power Systems and Clean Energy 4 (2) (2016) 161–179.

[7] H.Bevrani, A. Ghosh, G. Ledwich, Renewable energy sources and frequency regulation: survey and new perspectives, IET Renewable Power Generation 4 (5) (2010) 438–457.

[8] D. Greenwood, K. Y. Lim, C. Patsios, P. Lyons, Y. S. Lim, P. Taylor, Frequency response services designed for energy storage, Applied Energy 203 (2017) 115–127.

[9] Y. Xu, C. Li, Z. Wang, N. Zhang, B. Peng, Load frequency control of a novel renewable energy integrated micro-grid containing pumped hydropower energy storage, Ieee Access 6 (2018) 29067–29077.

[10] N. Vafamand, M. H. Khooban, T. Dragi˘cevi´ c, J. Boudjadar, M. H. Asemani, Time-delayed stabilizing secondary load frequency control of shipboard microgrids, IEEE Systems Journal 13 (3) (2019) 3233–3241.

[11] M. Vidi´c, I. Ba˘ ckalov, An analysis of stability requirements for large inland passenger ships, Ocean Engineering 261 (2022) 112148.

[12] M.-H. Khooban, T. Dragicevic, F. Blaabjerg, M. Delimar, Shipboard microgrids: A novel approach to load frequency control, IEEE Transac tions on Sustainable Energy 9 (2) (2017) 843–852.

[13] F. Shariatzadeh, N. Kumar, A. K. Srivastava, Optimal control algorithms for reconfiguration of shipboard microgrid distribution system using intelligent techniques, IEEE Transactions on Industry Applications 53 (1) (2016) 474–482.

[14] Z. Jin, G. Sulligoi, R. Cuzner, L. Meng, J. C. Vasquez, J. M. Guerrero, Next-generation shipboard dc power system: Introduction smart grid and dc microgrid technologies into maritime electrical netowrks, IEEE Electrification Magazine 4 (2) (2016) 45–57.

[15] A. Maleki, A. Askarzadeh, Optimal sizing of a pv/wind/diesel system with battery storage for electrification to an o-grid remote region: A case study of rafsanjan, iran, Sustainable Energy Technologies and Assessments 7 (2014) 147–153.

[16] G. Magdy, A. Bakeer, M. Nour, E. Petlenkov, A new virtual synchronous generator design based on the smes system for frequency stability of low-inertia power grids, Energies 13 (21) (2020) 5641.

[17] G. Magdy, G. Shabib, A. A. Elbaset, Y. Mitani, Renewable power systems dynamic security using a new coordination of frequency control strategy based on virtual synchronous generator and digital frequency protection, International Journal of Electrical Power & Energy Systems 109 (2019) 351–368.

[18] D.Chaturvedi, P. Satsangi, P. Kalra, Load frequency control: a generalised neural network approach, International Journal of Electrical Power &Energy Systems 21 (6) (1999) 405–415.

[19] H.Luo, Z.Hu, Stability analysis of sampled-data load frequency control systems with multiple delays, IEEE Transactions on Control Systems Technology 30 (1) (2021) 434–442.

[20] S. Wen, X. Yu, Z. Zeng, J. Wang, Event-triggering load frequency control for multiarea power systems with communication delays, IEEE Transactions on Industrial Electronics 63 (2) (2015) 1308–1317.